Available online at www.sciencedirect.com
SCIENCE DIRECT
Remote Sensing of Environment 100 (2006) 503 – 511
Remote Sensing of Environment
www.elsevier.com/locate/rse

Predicting lidar measured forest vertical structure from multi-angle spectral data

D.S. Kimes [a,*], K.J. Ranson [a], G. Sun [b], J.B. Blair [c]

[a] Biospheric Science Branch, NASA/Goddard Space Flight Center, Code 614.4, Greenbelt, MD 20771, USA
[b] Department of Geography, University of Maryland, College Park, MD 20742, USA
[c] Laser Remote Sensing Laboratory, NASA/Goddard Space Flight Center, Code 694.0, Greenbelt, MD 20771, USA

Received 8 June 2005; received in revised form 7 November 2005; accepted 12 November 2005

Abstract

A capability to remotely measure the vertical and spatial distribution of forest structure is required for more accurate modeling of energy, carbon, water, and climate over regional, continental, and global scales. We examined the potential of using a multi-angle spectral sensor to predict forest vertical structure as measured by an airborne lidar system. Data were acquired from AirMISR (Airborne Multi-Angle Imaging Spectrometer) and airborne LVIS (Laser Vegetation Imaging Sensor) for a 7000 ha study site near Howland Maine, consisting of small plantations, multi-generation clearings and large natural forest stands. The LVIS data set provided a relatively direct measure of forest vertical structure at a fine scale (20 m diameter footprints). Multivariate linear regression and neural network models were developed to predict the LVIS forest energy height measures from 28 AirMISR multi-angle spectral radiance values. The best model accurately predicted the maximum canopy height (as measured from LVIS) using AirMISR data (rmse = 0.92 m, $R^2 = 0.89$). The models developed in this study achieved high accuracies over a study site with an elaborate patchwork of forest communities with exceptional diversity in forest structure. We conclude that models using MISR-like data are capable of accurately predicting the vertical structure of forest canopies.
Published by Elsevier Inc.

Keywords: Forest vertical structure; Lidar; Multi-angle; Spectral; AirMISR; LVIS

1. Introduction

Forest structure affects the fluxes of energy and matter across the land–atmosphere interface, and the biodiversity of ecosystems. Forest structure is determined by several factors, including species composition and the three-dimensional distribution of leaves/needles and woody biomass. Many processes, both anthropogenic and non-anthropogenic, alter forest structure including forest management, natural disturbances, and recovery from disturbance (i.e., successional status or age class).

Most remote sensing systems, although providing images of the horizontal extent of canopies, do not provide direct information on the vertical distribution of canopy elements. For example, MODIS (Moderate Resolution Imaging Spectroradiometer) land products provide typical forest parameters at large spatial scales (e.g., forest type, %cover, leaf area index, and net primary production) (Justice & Townshend, 2002), but these products do not provide much insight into the vertical and spatial structure of the forest. Structural information is essential for realistic energy budgeting, and carbon and water cycle modeling at the landscape scale. This requires a capability to remotely measure the vertical and spatial distribution of forest structural parameters that are needed for more accurate models of energy, carbon, and water flux over regional, continental, and global scales. Lidars, multiangle radiometers, radars and imaging spectrometers have been identified as systems that can capture information in the vertical dimension (e.g. Dobson et al., 1996; Lefsky et al., 1999a; Ranson et al., 1994; Treuhaft et al., 2002). In this paper, we consider the use of lidars and multiangle radiometers to estimate forest vertical structure.

The composite return from a lidar footprint is called the lidar waveform signature. The lidar waveform from a large-footprint lidar instrument, such as the Laser Vegetation Imaging Sensor

* Corresponding author. Tel.: +1 301 614 6660.
E-mail address: dan@pika.gsfc.nasa.gov (D.S. Kimes).

0034-4257/$ - see front matter. Published by Elsevier Inc.
doi:10.1016/j.rse.2005.11.004

(LVIS) (Blair et al., 1999; Drake et al., 2002), has been successfully used to estimate the canopy height, stand volume, basal area, and above-ground biomass (Drake et al., 2002; Lefsky et al., 1999b; Means et al., 1999). The waveform data provides a relatively direct measure of the vertical profile of the canopy components (Blair & Hofton, 1999). In addition, LVIS has a high density of footprints across a wide swath (2 km) that can be used to form an image. LVIS data provide forest structure information and are an excellent data set for developing and testing methods to extract forest structure information using other kinds of sensor data. Ground data of forest structure at such a fine scale and for large regions has not been previously available for developing forest structure algorithms. In addition, lidars in orbit and proposed, do not have a continuous mapping capability, and provide only sample data in a region. A capability to continuously map the vertical structure for large regions would provide fundamental information that would enable more accurate modeling of energy, carbon, water, and climate (Landsberg & Waring, 1997; Cuevas, 2003; Dai et al., 2003; Engel et al., 2002; Hudak et al., 2002; Shugart, 2000).

Imaging the Earth's surface through various angles by the Multiangle Imaging Spectrometer (MISR) instrument on-board the Terra Spacecraft (Diner et al., 1998) could provide a capability to continuously map forest vertical structure by using directional reflectance information. Early studies showed the promise of directional reflectance data for distinguishing forest types (e.g., Ranson et al., 1994; Russell et al., 1997). Multi-angle data significantly improved the accuracy of recovering forest parameters when inverting 3-D optical models (Kimes et al., 2002). More recently, studies by the MISR science team members indicate the usefulness of off-nadir data for surface heterogeneity and vegetation structure (e.g., Chopping et al., 2003; Gobron et al., 2002; Jin et al., 2002; Pinty et al., 2002).

MISR's 375 km swath and 275–1100 m spatial resolutions may provide a capability of mapping forest structure parameters at regional, even global scales. Coincident data acquired from the MISR airborne simulator instrument (AirMISR web site) and LVIS provide an opportunity for examining the potential of using multi-angle spectral sensors to map forest vertical structure measures. In this study we explore the potential of accurately predicting forest vertical structure as measured from LVIS using AirMISR spectral and angular data. We developed and compared a number of prediction methods including linear and neural network models.

2. Methods

2.1. Study area

LVIS and AirMISR data were acquired in the summer of 2003 as part of a NASA Terrestrial Ecology Program aircraft campaign. Our study site is located at approximately 45° 15′N latitude and 68° 45′ W longitude at International Paper's Northern Experimental Forest near Howland, Maine, USA (Fig. 1). This site was also the location of the NASA Forest Ecosystem Dynamics Multi-sensor Aircraft Campaign in 1990 (Ranson et al., 1994; Ranson & Sun, 1994) and intensive SIR-C/XSAR (Spaceborne Imaging Radar-C/X-Band Synthetic Aperture Radar) experiments in 1994 (Ranson & Sun, 1997). The area comprises approximately 7000 ha containing several intensive experimental sites, where detailed ecological measurements have been obtained. The study area contains an assortment of small plantations, multi-generation clearings, and large natural forest stands. A variety of forest ecosystem studies are currently in progress at this site (e.g., Xiao et al., 2004).

The natural stands in this boreal-northern hardwood transitional forest consist of hemlock-spruce-fir, aspen-birch, and hemlock-hardwood mixtures. Topographically, the region varies from flat to gently rolling, with a maximum elevation change of less than 135 m within the 10 by 10 km study area. Due to the region's glacial history, soil drainage classes within a small area may vary widely, from excessively drained to poorly drained. Consequently, an elaborate patchwork of forest communities has developed, supporting exceptional diversity in forest structure (Ranson & Sun, 1997).

The soils are predominantly glacial tills; acid in reaction, low in fertility and high in organic matter. The majority of soils fall into the suborders orthods, orchrepts, or aquepts. Approximately 450 ha of the forest area is covered with bogs and wetlands in the central portion of the study site. There is also an excessively well-drained esker in this area. The variable nature of the soils (changing between very well drained to very poorly drained soils over a short distance) has produced irregular stand sizes and shapes. Wet areas are abundant and cause diversity of species and stand densities over small areas. The climate is cold, humid and continental with continuous snow pack from

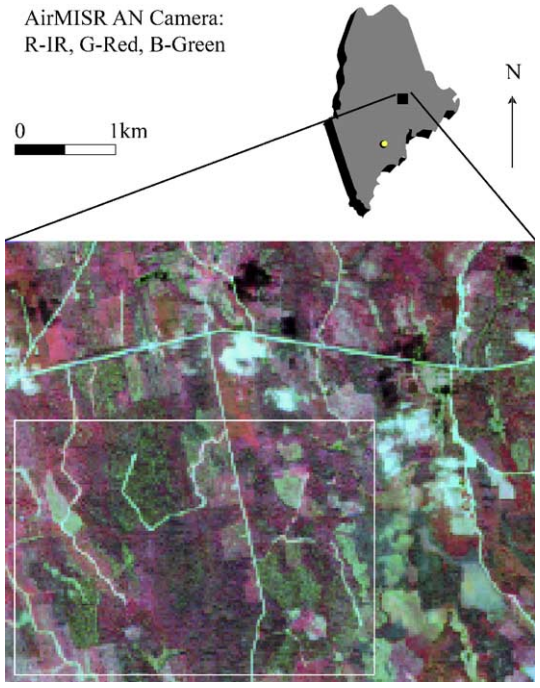

Fig. 1. AirMISR nadir color composite image of the study site near Howland, Maine. The white box is the cloud free area of the image. Within the white box, the green areas are roads or recent clear cut areas. The dark areas are conifer forests and the bright red areas are deciduous forests.

December through March with accumulations of 1 to 2 m (Ranson & Sun, 1997).

2.2. Field measurements

The Howland, Maine site has been the subject of several field measurement activities (e.g., see http://fedwww.gsfc.nasa.gov). During October 2003 the site was visited and twenty forest stands were measured. In each stand four 4 m radius plots were established with one plot located around a center point, and three other plots located 30 m to the north (0°), 30 m to the southeast (120°) and 30 m to the southwest (240°) of the center point. A total of 70 plots were measured. Global positioning system (GPS) location, diameter breast height, and species of all trees in a plot, and the height of the tallest tree in the plot were measured using an ultrasonic range finder and an inclinometer.

2.3. LVIS data

NASA's Laser Vegetation Imaging Sensor (LVIS) is an airborne laser altimeter system designed, developed and operated by the Laser Remote Sensing Laboratory, Goddard Space Flight Center. In 2003, LVIS obtained sub-canopy and canopy-top topography data as well as canopy vertical structure information for forested sites in New England to generate the most detailed forest structural data sets currently available for these regions. The data used in this study is the Nominal 20 m-spaced LVIS Ground Elevation Data (Blair et al., 2004).

Measurements derived from the lidar waveforms were used to characterize the canopy vertical structure. First, various ranging points were extracted including the elevations of the lowest and highest detectable returns (above a threshold noise level) and the mean ground elevation and various energy quartile heights (Fig. 2). In this study, we focused on 4 quartile heights, H25, H50, H75, and H100 (Blair et al., 1999). H25 is the 25% quartile height and is calculated by subtracting the elevation at which 25% of the returned energy occurs from the ground elevation. H100 is the canopy height and is calculated by subtracting the elevation of the highest detectable return from the ground elevation.

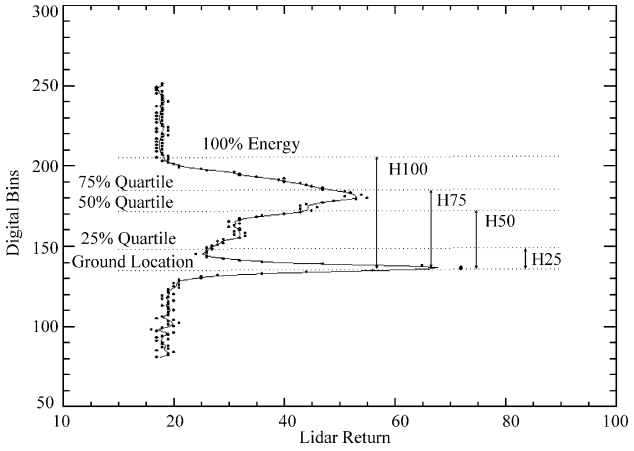

Fig. 2. LVIS return waveform showing ground, canopy (H100), and quartile heights (H75, H50, and H25). H100 is the location of the top of the canopy.

A typical forest waveform and the definition of these canopy structure measures are shown in Fig. 2. These quartile heights are a relatively direct measure of the vertical profile of canopy components. However, this is based on a number of assumptions including that multiple scattering effects are minimal, the ground and top of the canopy can be detected and accurately interpreted in terms of elevation, and a constant reflectance for all canopy components. In addition, waveform measures are a function of the complex and variable 3-D structure of canopy components and their spectral properties including the spectral properties of the ground/litter. This 3-D structure defines the gap distribution as a function of canopy height which largely determines the proportion of energy reaching a given height. This gap distribution, along with the spectral properties of the components, largely determines the proportion of energy scattered at a given height. Finally, the gap distribution largely determines the amount of scattered energy at a given height that returns to the sensor.

LVIS data provided continuous coverage of the study site. Fig. 3 presents LVIS images of the study site for these 4 vertical structure measures. These combined data contain detailed, continuous, spatial (20 m diameter footprints) information of the vertical distribution of forest canopy components for the study site. The heterogeneous nature of the site is clear for the different canopy elevations. Prior to 2002, the two circled regions in each image were relatively similar homogeneous stands of spruce and hemlock. In 2002, the white circle was selectively logged removing about 30% of the trees. Fig. 3 shows these stands after logging in 2003.

2.4. AirMISR data

The Airborne Multi-Angle Imaging Spectrometer (AirMISR) is a four channel digital camera that flies on the high altitude ER-2 aircraft. The four channels employed on AirMISR are 446.4 nm (blue), 557.5 nm (green), 671.7 nm (red), 866.4 nm (near-IR), with bandwidths of 41.9 nm, 28.6 nm, 21.9 nm, 39.7 nm, respectively. The AirMISR camera uses a MISR brassboard lens and a MISR engineering model focal plane; giving the airborne sensor spectral and radiometric characteristics very similar to the satellite instrument. AirMISR is a 'pushbroom' sensor, which images a cross-track slit beneath the aircraft during each scan. A two dimensional scene is built up by successive scans as the spacecraft or aircraft moves over the scene. The Satellite instrument, MISR, has nine cameras which image the earth continuously, however, AirMISR has a single camera that is swiveled to 9 successive look angles from 70.5° looking forward of the aircraft through nadir then out 70.5° looking aft of the aircraft (Table 1) as the aircraft passes over the site of interest.

The AirMISR data used here were acquired between 16:20 and 16:33 GMT on August 28, 2003. Fig. 1 shows a nadir color composite image of the site. Cloud cover was estimated to be less than 30% cumulus for the duration of the flight line. Mean solar zenith angle was 36° and mean solar azimuth angle was about 176°. The azimuth orientation of the flight line was about 0° with the sun oriented to the back of the aircraft.

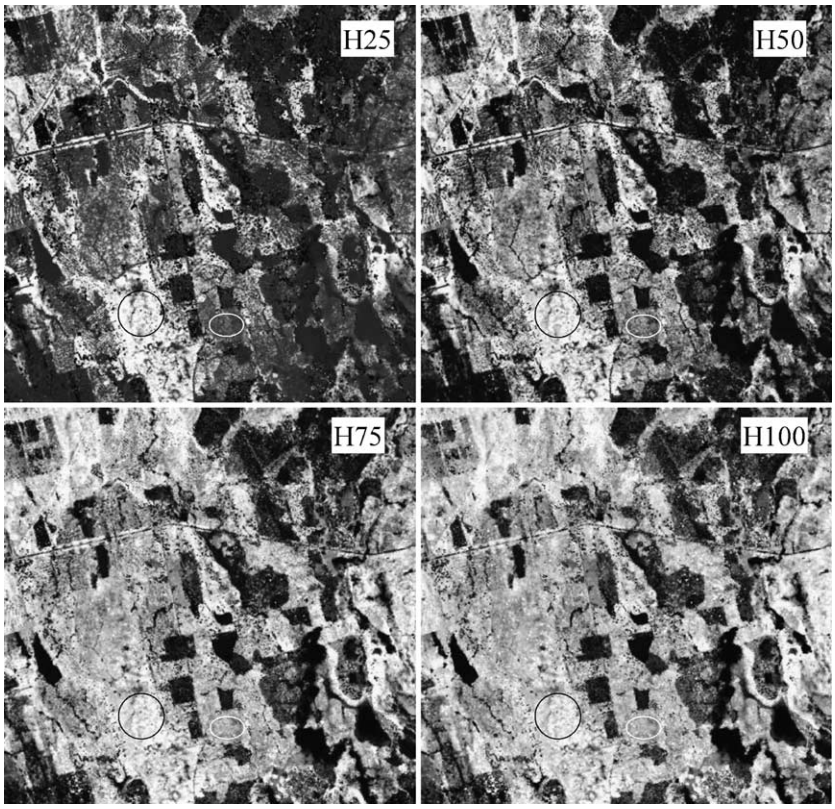

Fig. 3. LVIS images of the study site in 2003 for the 4 canopy vertical structure measures, a) H25, b) H50, c) H75, and d) H100. Dark to light shading corresponds to low to high LVIS values, respectively. The two circled areas (one black and one white) show two stands of spruce and hemlock that were similar prior to 2002. The white circle area was selectively logged in 2002.

Consequently, the AirMISR data was collected within approximately 4° of the solar azimuth plane. The forward looking camera (f) acquires backscattered radiance and the aft looking camera (a) acquires forward scattered radiance (Table 1). The aircraft flew at about 20 km altitude providing view angle dependent variable ground spatial resolutions and swath widths (Table 1). The data were normalized to a common resolution of 27.5 m and co-registered to a common swath width of 11 km by the AirMISR Project (AirMISR web site).

2.5. Data processing and analysis

The AirMISR image data set was co-registered with an ASTER (Advanced Spaceborne Thermal Emission and Reflection Radiometer) image (Yamaguchi et al., 1998) and resampled into the 15 m nominal pixel size of ASTER. The ASTER images were used in this study because they were used as the base map as part of a larger multi-sensor data fusion study. LVIS point data were gridded to the 15×15 m pixels corresponding to the 15 m AirMISR and ASTER data.

The LVIS H100 height measures were compared to maximum tree heights as measured on the ground. Because the ground measured footprint (4 m radius) and the LVIS footprints (10 m radius) never overlay exactly, this comparison is far from ideal. Various comparisons were tested. We report a comparison between the maximum tree height for the 70 field plots and the corresponding mean of the 4 nearest LVIS H100 values (weighted by the inverse distance to the to the field plot center) in the Results and discussion section.

Table 1
Ground characteristics of AirMISR pixels for each camera angle where *D, C, B,* and *A*, represent the different camera angles and *f*, *a*, and *n* represent the forward, aft, and nadir looking directions, respectively, relative to the aircraft flight line

Ground characteristics	Camera angle				
	Df, *Da* ±70.5°	*Cf*, *Ca* ±60°	*Bf*, *Ba* ±45.6°	*Af*, *Aa* ±26.1°	*An* 0°
Swath width (km)	32.7	21.8	15.6	12.1	10.9
Along track image length (km)	27.0	17.0	11.3	9.6	9.6
Cross track pixel size (m)	21.7	14.5	10.4	8.1	7.3
Along track pixel size (m)	55.8	24.9	12.7	7.7	6.2
Line spacing (distance traveled between scans)	8.3 m, for all angles				
%Overlap/Underlap (gap)	85%	67%	35%	−8%	−34%

Models were developed to predict LVIS quartile height measures from AirMISR data. The 4 closest LVIS shots to the center point of a pixel were identified. All calculations used the center of each pixel and the center of the 4 closest LVIS shots. The averages of the H25, H50, H75, and H100 values of these 4 closest LVIS shots (weighted by the inverse distance) were calculated for each pixel. A random sample of 1000 points was selected over the cloud free portion of the study area (identified as the white box in Fig. 1.). The cloud free area was determined by visual inspection of the multi-angle, color composite images from AirMISR. The mean LVIS quartile height measures and the mean spectral AirMISR radiances within a 3×3 pixel window were calculated for each random point where the point falls within the center pixel of the 3×3 pixel window. The *Da* (aft looking 70.5°) and *Df* (forward looking 70.5°) camera data of AirMISR were not used because of poor spatial resolution and co-registration with data of other angles. Consequently, 28 AirMISR radiance values were available. A similar procedure was applied to the random sample points using 1000 9×9 pixel windows and 1000 17×17 pixel windows. These larger windows were explored to see if the accuracies in predicting the forest structure using AirMISR data changes with increasing window size. The larger windows averaged more LVIS shots and, consequently, were more representative of an area. The results focused on these 3×3, 9×9, and 17×17 pixel windows.

The effects of additional noise in the multi-angle spectral radiances on the model accuracies were explored as follows. For a selected model with its particular multi-angle spectral inputs, 11 noise levels were generated and added to the input radiances of the test data and the accuracy of the model was then tested. Eleven noise levels from 0% to 5% of the true signal were defined. To generate these data, random error was added to each directional reflectance, e.g. $R'_\lambda = R_\lambda + ((E * R_\lambda)/2)$ where E is the random error uniformly distributed within the noise level specified (±0–5%). The model's predictions were then performed using the R'_λ values. These noisy data sets were presented to the linear and neural network models (trained on error free data), and the rmse (root mean square error) values were calculated between the true and predicted forest structure measures. The increasing error in the predicted forest structure measures with increasing noise in the spectral/direction data was then graphically displayed.

2.6. Models

Multivariate linear regression and neural networks models were developed to predict the LVIS height measures from the 28 AirMISR radiance values. The accuracies of the models were compared. Two statistics were calculated for each model for the purpose of documenting and comparing model accuracies. These statistics were the rmse (root mean square error of the predicted versus true target value of the model) and the R^2 (coefficient of determination of the predicted versus true target value of the model). For all analyses, the dataset was partitioned into training and testing sets. In all cases, 1000 points were chosen randomly from the data set for training/fitting and another 1000 points were chosen randomly from the data set for testing. The points correspond to the center of the window pixels, e.g., 3×3, 9×9, or 17×17 windows. The test data was used to see how well the model generalized to independent data sets. These random points were chosen over the cloud free portion of the study area (white box in Fig. 1).

The neural networks (NN) were chosen for several reasons. NN employ a more powerful and adaptive nonlinear equation form than traditional linear and simple nonlinear analyses. In using traditional approaches, one adopts linear or simple nonlinear forms that must be explicitly designed by a researcher. In contrast, a NN adaptively develops its own basis functions, and their corresponding coefficients from the collected data. NNs attempt to find the best nonlinear function based on the network's complexity without the constraint of linearity or pre-specified nonlinearity. This allows the NNs to learn complex functional relationships that cannot be envisioned by a researcher (Kimes et al., 1998).

Fu (1994), Hagan et al. (1995), Kimes et al. (1998) present an overview of the architectures, learning rules, and mathematical analyses of neural networks and their applications. In this study a cascade method of network construction (Fahlmann & Lebiere, 1988) was used that adds a hidden node one at a time during its training phase. As each hidden node is added it is fully connected to all previous nodes. Once a hidden node is added and trained, its weights are fixed. The advantages to this type of network are that it learns very quickly, determines its own network size, and seems to be relatively robust in learning complex mapping functions relevant to this study (Kimes et al., 1998). Several methods were used to avoid over-fitting the training data including reducing network structure, halting training when test performance began to decline, and decreasing the number of input variables. The activation function used for the hidden nodes was the hyperbolic tangent function and for the output node was the sigmoid function.

Not all of the input data were necessary to give the best accuracy for the NN models. An exhaustive search for the subset of the 28 AirMISR inputs that resulted in the highest NN accuracy was conducted. These "best" combinations were the most accurate multi-angle spectral combinations for predicting the LVIS height measures. The input variables can interact in a highly nonlinear fashion. A particular directional view and spectral band were added only if they significantly increased the accuracy of prediction.

3. Results and discussion

A comparison was made between the maximum tree heights as measured on the ground for the 70 field plots and the corresponding average of the 4 nearest LVIS H100 values (weighted by the inverse distance to the field plot). A simple regression between the ground measured maximum tree height and LVIS H100 had an rmse and R^2 of 3.4 m and 0.55, respectively. These results were improved by using all of the LVIS height measures (H100, H75, H50, H25) to predict the ground measured maximum height. The best model had an

Table 2
Testing accuracy for selected models for predicting LVIS H100 values from AirMISR variables for the 3 × 3, 9 × 9, and 17 × 17 pixel windows

Model	Inputs	Structure	rmse	R^2
ML-3 × 3-17	All inputs except: *CaR, BaIR, BaR, BaG, BaB, AaIR, AaB, AnR, AfR, BfR, BfG*	17 → 1	2.90 m	0.48
NN-3 × 3-13	*CaIR, CaR, CaB, BaIR, BaB, AaG, AaB, AnR, AnG, AfIR, AfG, AfB, CfG*	13 → 10 → 1	2.78 m	0.52
ML-9 × 9-18	All inputs except: *BaIR, BaB, AaB, AnIR, AfIR, AfR, BfIR, BfR, BfG, CfIR*	18 → 1	2.00 m	0.66
NN-9 × 9-8	*CaIR, CaR, AnIR, AnG, AfR, AfG, BfB, CfG*	8 → 12 → 1	1.81 m	0.71
ML-17 × 17-22	All inputs except: *BaIR, AaIR, IfIR, RfR, CfIR, CfR*	22 → 1	1.22 m	0.75
NN-17 × 17-15	*BaIR, BaB, AaG, AaB, AnIR, AnG, AnB, AfIR, AfR, AfG, BfIR, BfG, BfB, CfIR, CfR*	15 → 29 → 1	0.92 m	0.89

The inputs are the variables used by a particular model to make a prediction. The models are multivariate linear regression (ML) and neural network (NN) for 3 × 3, 9 × 9, and 17 × 17 pixel windows. The network structures are denoted as #input-nodes → #hidden-nodes → #output-nodes. The rmse (root mean squared error of the predicted versus true target value of the model) and the R^2 (coefficient of determination of the predicted versus true target value of the model). Each of the 28 inputs from AirMISR are represented as View-Angle (*D*, *C*, *B*, or *A*, as shown in Table 1), Forward/Aft/Nadir Looking (*f*, *a*, *or n*, respectively, as shown in Table 1), and spectral bands (*B*, *G*, *R*, and *IR*). For example, *CaIR* is the camera angle *C* (60°), aft looking (*a*), and the *IR* spectral band.

rmse and R^2 value of 1.9 m and 0.64, respectively. These accuracies are relatively low because the comparison is between the maximum tree height measured for each 4 m radius plot and the average LVIS H100 values of 4 nearby shots with 10 m radius diameter footprints. These accuracies demonstrate the difficulties in comparing ground measured heights with lidar measured heights when they do not measure the exact same footprint on the ground.

Table 2 shows the testing accuracies for selected models for predicting LVIS H100 values from the 28 AirMISR variables for the 3 × 3 pixel window. The best NN model (Table 2, model NN-3 × 3-13) had an rmse and R^2 of 2.78 m and 0.52, respectively, for the testing data. The best linear model (Table 2, model ML-3 × 3-17) had an rmse and R^2 of 2.90 m and 0.48, respectively, for the testing data. Although the results are focused on the LVIS H100 data, the accuracies in predicting the H75, H50, and H25 values were similar to those achieved for the H100 data.

The predictions of LVIS height measures from AirMISR variables using the 9 × 9 pixel window were higher than with the 3 × 3 pixel window (Table 2). For example, the best NN model for predicting H100 was NN-9 × 9-8 (Table 2) which had a testing rmse and R^2 of 1.81 m, and 0.71, respectively. Similar accuracies were obtained for H75, H50, and H25 values. The 9 × 9 pixel window accuracies were higher than the 3 × 3 pixel windows because a larger number of AirMISR pixels (81 vs. 9, respectively) were averaged together and a larger number of LVIS footprints (324 vs. 36, respectively) were averaged together resulting in a more accurate characterization of the variability within forest stands.

The predictions of LVIS height measures from AirMISR variables using the 17 × 17 pixel window obtained the highest accuracies. For example, the best model for predicting H100 was NN-17 × 17-15 (Table 2) which had a testing rmse and R^2 of 0.92 m, and 0.89, respectively. Similar accuracies were obtained for H75, H50, and H25 values; for example, the testing rmse were 1.0, 1.0, and 0.83, respectively, and the R^2 values were 0.85, 0.81, and 0.79, respectively. Fig. 4 shows a graph of the true versus predicted LVIS H100 values (testing data only).

The best NN and ML models (Table 2) included a wide range of view angles in the forward, aft, and nadir looking directions as well as all spectral bands (*IR, B, G,* and *R*). A number of NN models were developed that utilized a smaller number of inputs. These models were developed to examine which combinations of view-angle and spectral bands were critical in predicting the LVIS H100 value accurately. Because of the high overall accuracies of the 17 × 17 window data, this window size was used for these analyses. Table 3 shows the testing accuracy for these selected NN models. The most accurate model NN-17 × 17-15 used 15 variables and had an rmse and R^2 value of 0.92 m and 0.89, respectively (this is the same model in Table 2 for comparison). As the number of allowed input variables was reduced, the accuracy remained high even with only 5 variables (Table 3, Model NN-17 × 17-5, rmse = 1.11 m, and R^2 = 0.84). This model used the 45.6° aft looking near infrared band, the 26.1° aft looking red band, and the 26.1° forward looking red band, and the 60° forward looking green and blue bands. The models using less than 5 input variables had relatively low accuracies (Table 3).

The models accurately predict the forest vertical structure in a 17 × 17 pixel window (255 × 255 m). These accuracies were high in a study site that is a relatively heterogeneous area consisting of small plantations, multi-generation clearings and large natural forest stands. In addition, the forest stands consist of hemlock-spruce-fir, aspen birch, and hemlock-hardwood mixtures. Further more, as mentioned previously, the soil drainage classes vary widely from excessively drained to

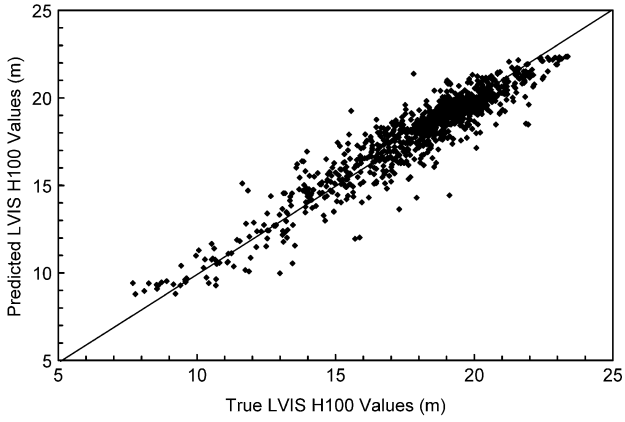

Fig. 4. Predicted versus true LVIS H100 heights for the 17 × 17 pixel windows using model (Table 2, Model NN-17 × 17-15). The model was applied to 1000 random test points.

Table 3
Testing accuracy for selected models for predicting LVIS H100 values from AirMISR variables (17 × 17 pixel windows)

Model	Inputs	Structure	rmse	R^2
NN-17 × 17-15	*BaIR*, *BaB*, *AaG*, *AaB*, *AnIR*, *AnG*, *AnB*, *AfIR*, *AfR*, *AfG*, *BfIR*, *BfG*, *BfB*, *CfIR*, *CfR*	15→29→1	0.92 m	0.89
NN-17 × 17-7	*BaIR*, *AnG*, *AfG*, *BfB*, *CfG*, *CfB*, *CfR*	7→28→1	1.09 m	0.84
NN-17 × 17-5	*BaIR*, *AaR*, *AfR*, *CfG*, *CfB*	5→29→1	1.11 m	0.84
NN-17 × 17-4	*BaR*, *AaG*, *RfG*, *BfB*	4→25→1	1.49 m	0.71
NN-17 × 17-3	*AfG*, *AfB*, *BfIR*	3→18→1	1.68 m	0.64
NN-17 × 17-2	*BaIR*, *AfR*	2→10→1	1.69 m	0.63
NN-17 × 17-1	*AfG*	1→1	1.93 m	0.52

The table headings follow Table 1. In a similar fashion the neural network model NN-17 × 17-15 allowed any combination of AirMISR variables as inputs and used 15 input variables. Each successive NN model reduced the number of inputs allowed in predicting LVIS H100.

poorly drained causing an elaborate patchwork of forest communities with exceptional diversity in forest structure (Ranson & Sun, 1997). Even though a relatively heterogeneous mixture of cover-types and structure occur within a window, the models using the average of multi-angle spectral AirMISR data provide an accurate prediction of the average LVIS height measures for the same area.

The atmospheric scattering in the blue band introduces a large noise component at higher altitudes (aircraft and satellite levels). Several models were developed that did not use the blue band. The results showed that approximately the same level of accuracy could be obtained without using the blue band. For example, a network using 5 input variables (*CaIR, CaR, AnIR, AfG, CfR*) had an rmse and R^2 of 1.2 and 0.79, respectively, and the network structure was 5→27→1. This model has essentially the same accuracy (rmse = 1.1) as model NN-17 × 17-5 (Table 3) that uses the blue band and 5 inputs.

Next, we explored models that were allowed to only use nadir spectral values. A NN model with only the spectral nadir values (*AnIR, AnB, AnG, AnR*) available had an rmse and R^2 value of 1.77 and 0.59, respectively (Table 4, Model NN-17 × 17-S). This low accuracy demonstrates that for this case study, forest vertical structure can not be accurately captured using only spectral information.

Finally, we explored models that were allowed to use all view angles but only a single spectral band. A NN model with all view angles available and only the IR band (*CaIR, BaIR, AaIR, AnIR, AfIR, BfIR, CfIR*) had an rmse and R^2 value of 1.98 and 0.49, respectively (Table 4, Model NN-17 × 17-D1). In a similar fashion, a NN model with all view angles available and only the Red band had an rmse and R^2 value of 1.80 and 0.58, respectively (Table 4, Model NN-17 × 17-D2). These low accuracies demonstrate that for this case study, forest vertical structure can not be accurately captured using only directional data for the 17 × 17 pixel windows. It seems that both multi-angle and spectral data are necessary to obtain higher accuracies (Table 3).

Table 4
Testing accuracy for selected models for predicting LVIS H100 values from AirMISR variables (17 × 17 pixel windows)

Model	Inputs	Structure	rmse	R^2
NN-17 × 17-S	*AnIR*, *AnR*, *AnG*, *AnB*	4→19→1	1.77 m	0.59
NN-17 × 17-IR	*BaIR*, *AaIR*, *AnIR*, *AfIR*,	4→2→1	1.98 m	0.49
NN-17 × 17-R	*CaR*, *BaR*, *AaR, An, AfR, CfR*	6→30→1	1.80 m	0.58

The table headings follow Table 1. The neural network model NN-17 × 17-S allowed inputs of any spectral band in the nadir direction. The NN-17 × 17-IR model allowed inputs of any directional view for the IR band only. The NN-17 × -17R model allowed inputs of any directional view for the Red band only.

The results of this study demonstrate the ability to extract forest structure information using multi-angle spectral AirMISR data. This kind of information can be used to identify subtle differences in forest structure that are of importance to biomass, carbon, and ecosystem disturbance studies. For example, Fig. 3 shows two circled regions in each image that were relatively similar homogeneous stands of spruce and hemlock prior to 2002. In 2002, the smaller circle was selectively logged removing about 30% of the trees. Fig. 3 shows these stands in 2003 after logging.

The H100 image in Fig. 3 shows that the maximum height of the logged area is similar to the unlogged area, although the logged area is slightly darker representing a slightly lower maximum height. As one moves from the H100, H75, H50 and H25 images, the logged area becomes progressively darker relative to the unlogged area. In other words, as one proceeds from the top of the canopy to the ground, more pulse energy is returned to the sensor in the logged area relative to the unlogged area. For example, the height at which 25% of the energy is returned (H25) is much lower (closer to the ground) in the logged area relative to the unlogged area. The logged forest allows greater penetration of the laser pulse into the

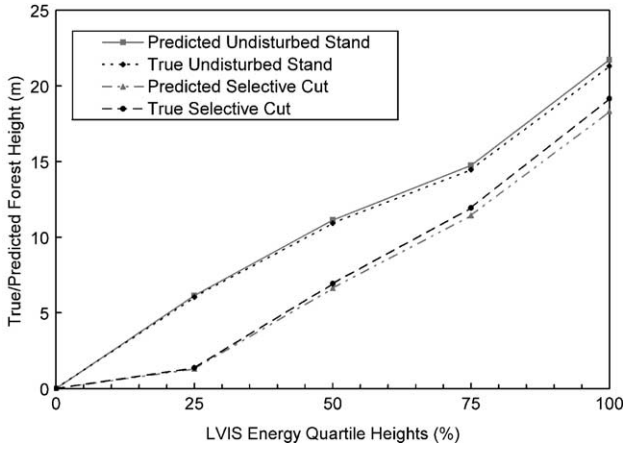

Fig. 5. Predicted versus true LVIS energy for canopy height (H100) and quartile heights (H75, H50, H25) for the logged and unlogged areas (Fig. 3). The predictive models used only AirMISR data and used the 17 × 17 pixel windows.

forest canopy and a larger proportion of the energy is returned from deeper into the canopy.

Using the models developed in this study for the 17×17 pixel windows, we predicted the energy quartile heights using AirMISR data and compared these predicted values with the true quartile height values as measured from LVIS data. Fig. 5 shows the average predicted and true quartile heights for the logged and unlogged areas. The predicted and true values are very close for both logged and unlogged areas. The figure clearly shows that as one proceeds from the top of the canopy to the ground, for any given height, a significantly higher proportion of pulse energy is returned to the sensor from objects below this level (canopy components and ground) for the logged area relative to the unlogged area. Thus, for any specific quartile height, it occurs at a significantly lower canopy height for the logged area (Fig. 5). These trends are most exaggerated at the 25% quartile height.

These kinds of vertical structural measures have many applications. For example, the H50 value has been shown to be a good single variable predictor of forest biomass by Drake et al. (2002). Forest structure measures have also been successfully used to estimate the canopy stand volume and basal area (Lefsky et al., 1999b; Means et al., 1999). In addition, structural information may improve vegetation cover mapping and vegetation disturbance identification (as demonstrated above) for many applications.

Are these models of forest structure using a multi-angle spectral sensor data applicable to current and future satellite data (e.g., MISR)? Currently, the authors are exploring and developing relationships with MISR data. However, in this study we explored how sensitive these models using AirMISR data are to noise. As described in the Data processing and analysis, the addition of noise in each multi-angle spectral input variable provided information on how sensitive the models would be to noise introduced from other sources such as atmospherically corrected data. Fig. 6 shows how the errors increase with increasing noise in the multi-angle spectral input for selected models. These models have about the same level of sensitivity to noise. The models are relatively sensitive to noise with the rmse value approximately doubling with each 2% increase in noise. However, it should be noted that the data set used in this study already contains a significant amount of noise due to atmospheric variations due to thin clouds as well as instrument noise (both AirMISR and LVIS).

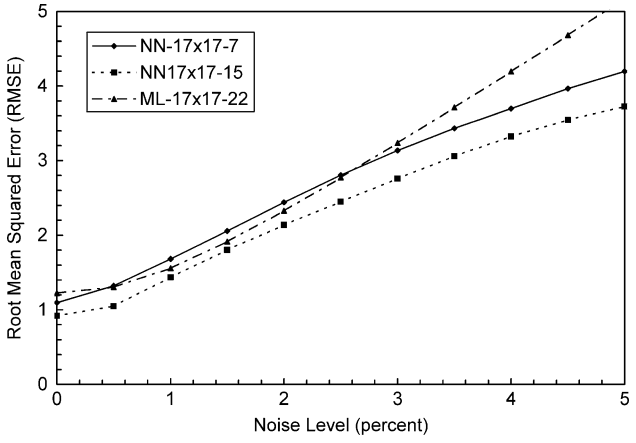

Fig. 6. Root mean squared error of LVIS H100 prediction as a function of noise level in the multi-angle spectral radiance data. Various selected models are shown (Tables 2 and 3).

4. Conclusions and implications

The models developed in this study achieved high accuracies over a study site with an elaborate patchwork of forest communities with exceptional diversity in forest structure. Models using the 17×17 window had high accuracies when predicting the H100 value (rmse = 0.92 m, $R^2 = 0.89$) using 15 inputs (all view angles and all spectral bands). The accuracies for predicting the H75, H50, and H25 values had similar accuracies.

Relatively high accuracies were obtained with models using a minimum number of inputs. For example, Models using the 17×17 window data with only 5 inputs (4 view angles and 4 spectral bands) had accuracies of rmse = 1.11 m, $R^2 = 0.84$. At the satellite level, the blue band is not appropriate for retrieving canopy parameters due to the large atmospheric scattering component; however, high accuracies were obtained without this band. In this study, forest vertical structure can not be captured accurately using only the 4 spectral bands in the nadir view or all view angles with a single spectral band.

These methods seem to be relatively accurate even at the highest canopy density experienced in this study that was estimated at 300 t/ha. In addition, these models are relatively sensitive to noise with the rmse value approximately doubling with each 2% increase in noise. The authors are currently exploring the potential of using MISR data for predicting forest structure measures.

The data products from LVIS available at the time of this study were limited to the H100, H75, H50, and H25 quartile height values. We believe, however, that many other forest structure measures could be accurately estimated using multi-angle-spectral data. For example, these forest structure measures could provide additional information to accurately retrieve other key parameters such as biomass, leaf area index, fraction of photosynthetically active radiation, and albedo. In addition, forest structure information could be utilized as additional constraints for current retrieval/inversion algorithms (e.g. look-up-table approaches) for vegetation parameters.

It has been shown that the directional radiances in or near the principal plane of the sun provides information that leads to more accurate prediction of canopy structure parameters than from other azimuth planes (e.g., Gobron et al., 2000). For satellite data (e.g., MISR) the directional views deviate from the principal plane of the sun. Consequently, the authors believe that the accuracies for predicting forest structure measures may decrease as the deviation from the solar plane increases.

In conclusion, models similar to the ones developed in this study using MISR-like data are capable of accurately predicting the vertical structure of forest canopies. A continuous capability to remotely measure the vertical and spatial distribution of

forest structure is required for more accurate modeling of energy, carbon, water, and climate over large regional, continental, and global scales. The findings also provide information for future satellite and aircraft mission design.

Acknowledgments

This work was funded, in part, by NASA's Science Mission Directorate. The LVIS data were provided by the Laser Vegetation Imaging Sensor (LVIS) team in the Laser Remote Sensing Laboratory at NASA Goddard Space Flight Center with support from the University of Maryland, College Park. Funding for the collection and processing of the northeastern USA data was provided by NASA's Terrestrial Ecology Program (NASA Grant number NAG512112).

References

Airborne Multi-angle Imaging SpectroRadiometer (AirMISR) web site. http://www-misr.jpl.nasa.gov/mission/air.html

Blair, J. B., & Hofton, M. A. (1999). Modeling laser altimeter return waveforms over complex vegetation using high-resolution elevation data. *Geophysical Research Letters*, *26*, 2509–2512.

Blair, J. B., Rabine, D. L., & Hofton, M. A. (1999). The laser vegetation imaging sensor (LVIS): A medium-altitude, digitations-only, airborne laser altimeter for mapping vegetation and topography. *ISPRS Journal of Photogrammetry and Remote Sensing*, *54*, 115–122.

Blair, J. B., Hofton, M. A., Rabine, D. L. (2004). Processing of NASA LVIS Elevation and Canopy (LGE, LCE, and LGW) Data Products, Version 1.0. http://lvis.gsfc.nasa.gov

Chopping, M. J., Rango, A., Havstad, K. M., Schiebe, F. R., Ritchie, J. C., Schmugge, T. J., et al. (2003). Canopy attributes of desert grassland and transition communities derived from multiangular airborne imagery. *Remote Sensing of Environment*, *85*, 339–354.

Cuevas, J. G. (2003). Gap characteristics in relation to forest structure and implications for southern beech forest dynamics. *Canadian Journal Forest Research*, *33*, 1915–1922.

Dai, Y., Zeng, X., Dickinson, R. E., Baker, I., Bonan, G. B., Bosilovich, M.G, et al. (2003). The common land model (CLM). *Bulletin of the American Meteorological Society*, *84*, 1013–1023.

Diner, D. J., Beckert, J. C., Reilly, T. H., Bruegge, C. J., Conel, J. E., Kahn, R., et al. (1998). Multi-angle Imaging SpectroRadiometer (MISR) description and experiment overview. *IEEE Transactions on Geoscience and Remote Sensing*, *36*, 1072–1087.

Dobson, M. C., Pierce, L. E., & Ulaby, F. T. (1996). Knowledge-bases land-cover classification using ERS-1/JERS-1 SAR composites. *IEEE Transactions on Geoscience and Remote Sensing*, *34*, 83–95.

Drake, J. B., Dubayah, R. O., Clark, D. B., Knox, R. G., Blair, J. B., Hofton, M. A., et al. (2002). Estimation of tropical forest structural characteristics using large-footprint lidar. *Remote Sensing of Environment*, *79*, 305–319.

Engel, V. C., Stieglitz, M., Williams, M., & Griffin, K. l. (2002). Forest canopy hydrolic properties and catchment water balance: Observations and modeling. *Ecological Modeling*, *154*, 263–288.

Fahlmann, S., & Lebiere, C. (1988). The cascade-correlation learning architecture. In D. Touretzky*Advances in Neural Information Processing Systems*, *Vol. 2* (pp. 524–532). San Mateo, CA: Morgan Kaufmann.

Fu, L. (1994). Neural networks in computer intelligence. New York: McGraw-Hill, Inc. 460 pp.

Gobron, N., Pinty, B., Verstraete, M. M., Martonchik, J. V., Knyazikhin, Y., & Diner, D. J. (2000). Potential of multiangular spectral measurements to characterize land surfaces: Conceptual approach and exploratory application. *Journal of Geophysical Research*, *105*, 17539–17549.

Gobron, N., Pinty, B., Verstraete, M. M., Widlowski, J. L., & Diner, D. J. (2002). Uniqueness of multiangular measurements — Part II: Joint retrieval of vegetation structure and photosynthetic activity from MISR. *IEEE Transactions on Geoscience and Remote Sensing*, *40*, 1574–1592.

Hagan, M. T., Demuth, H. B., & Beale, M. (1995). Neural network design. Boston: PWS Publishing Company.

Hudak, A. T., Lefsky, M. A., Cohen, W. B., & Berterretche, M. (2002). Integration of lidar and Landsat ETM plus data for estimating and mapping forest canopy height. *Remote Sensing of Environment*, *82*, 397–416.

Jin, Y., Gao, F., Schaaft, C. B., Li, X., & Strahler, A. H. (2002). Improving MODIS surface BRDF/albedo retrieval with MISR multiangle observations. *IEEE Transactions on Geoscience and Remote Sensing*, *40*, 1593–1604.

Justice, C. O., & Townshend, J. (2002). Special issue on the Moderate Resolution Imaging Spectroradiometer (MODIS): A new generation of land surface monitoring (editorial). *Remote Sensing of Environment*, *83*, 1–2.

Kimes, D. S., Nelson, R. F., Manry, M. T., & Fung, A. (1998). Attributes of neural networks for extracting continuous vegetation variables from optical and radar measurements. *International Journal of Remote Sensing*, *19*, 2639–2663.

Kimes, D. S., Gastellu-Etchegorry, J., & Esteve, P. (2002). Recovery of forest canopy characteristics through inversion of a complex 3D model. *Remote Sensing of Environment*, *79*, 320–328.

Landsberg, J. J., & Waring, R. H. (1997). A generalized model of forest productivity using simplified concepts of radiation-use efficiency, carbon balance and partitioning. *Forest Ecology and Management*, *95*, 209–228.

Lefsky, M. A., Cohen, W. B., Acker, S. A., Parker, G. G., Spies, T. A., & Harding, D. (1999). Lidar remote sensing of the canopy structure and biophysical properties of Douglas-fir western hemlock forests. *Remote Sensing of Environment*, *70*, 339–361.

Lefsky, M. A., Harding, D., Cohen, W. B., Parker, G., & Shugart, H. H. (1999). Surface lidar remote sensing of basal area and biomass in deciduous forests of Eastern Maryland, USA. *Remote Sensing of Environment*, *67*, 83–98.

Means, J. E., Acker, S. A., Harding, D. J., Blair, J. B., Lefsky, M. A., Cohen, W. B., et al. (1999). Use of large-footprint scanning airborne lidar to estimate forest stand characteristics in the Western Cascades of Oregon. *Remote Sensing of Environmen*, *67*, 298–308.

Pinty, B., Widlowski, J. L., Gobron, N., Verstraete, M. M., & Diner, D. J. (2002). Uniqueness of multiangular measurements — Part I: An indicator of subpixel surface heterogeneity from MISR. *IEEE Transactions on Geoscience and Remote Sensing*, *40*, 1560–1573.

Ranson, K. J., Irons, J. R., & Williams, D. L. (1994). Multispectral bidirectional reflectance of northern forest canopies with ASAS. *Remote Sensing of Environment*, *47*, 276–289.

Ranson, K. J., & Sun, G. (1994). Northern forest classification using temporal multifrequency and multipolarimetric SAR images. *Remote Sensing Of Environment*, *47*, 142–153.

Ranson, K. J., & Sun, G. (1997). An evaluation of AIRSAR and SIR-C/X-SAR data for estimating northern forest attributes. *Remote Sensing of Environment*, *59*, 203–222.

Russell, C. A., Irons, J. R., & Dabney, P. W. (1997). Bidirectional reflectance of selected BOREAS sites from multiangle airborne data. *Journal of Geophysical Research-Atmospheres*, *102*(D24), 29505–2951.

Shugart, H. H. (2000). Importance of structure in the longer-term dynamics of landscapes. *Journal of Geophysical Research-Atmospheres*, *105*(D15), 20065–20075.

Treuhaft, R. N., Asner, G. P., Law, B. E., & Van Tuyl, S. (2002). Forest leaf area density profiles from quantitative fusion of radar and hyperspectral data. *Journal of Geophysical Research-Atmospheres*, *107*(D21) (Art. No. 4568).

Xiao, X. M., Hollinger, D., Aber, J., Goltz, M., Davidson, E. A., Zhang, Q. Y., et al. (2004). *Remote Sensing of Environment*, *89*, 519–534.

Yamaguchi, Y., Kahle, A. B., Kawakami, T., & Pniel, M. (1998). *IEEE Transactions on Geoscience and Remote Sensing*, *36*, 1062–1071.